VIP Metallopolymers Very Important Paper

How to cite: *Angew. Chem. Int. Ed.* **2023,** *62,* e202216060
International Edition: doi.org/10.1002/anie.202216060
German Edition: doi.org/10.1002/ange.202216060

Metal-Backboned Polymers with Well-Defined Lengths

Kaiwen Zeng[+], Yibei Yang[+], Jianing Xu, Ning Wang, Weiqiang Tang, Jianchen Xu, Yifeng Zhang, Yanruzhen Wu, Yifei Xu, Guowei Wang, Peining Chen, Bingjie Wang, Xuemei Sun, Guoxin Jin, and Huisheng Peng**

Abstract: Constructing the backbones of polymers with metal atoms is an attractive strategy to develop new functional polymeric materials, but it has yet to be studied due to synthetic challenges. Here, metal atoms are interconnected as the backbones of polymers to yield metal-backboned polymers (MBPs). Rational design of multidentate ligands synthesized via an efficient iterative approach leads to the successful construction of a series of nickel-backboned polymers (NBPs) with well-defined lengths and up to 21 nickel atoms, whose structures are systematically confirmed. These NBPs exhibit strong and length-depended absorption with narrow band gaps, offering promising applications in optoelectronic devices and semiconductors. We also demonstrate the high thermal stability and solution processsability of such nickel-backboned polymers. Our results represent a new opportunity to design and synthesize a variety of new metal-backboned polymers for promising applications in the future.

Metals and polymers are two important materials both in industry and in our daily life.[1] To meet a variety of application demands, many effective strategies on altering their components and structures have been made for achieving desirable properties.[2] For instance, adding small amounts of secondary elements for alloying[3] and mixing multiple high concentration metal elements to create high-entropy alloys[4] are two effective strategies to confer desirable properties to metallic materials. The strategies are more abundant for polymers by modulating the alternations such as the repeat units, chain lengths, stereoregularity and morphology.[5] However, these alternations are typically limited to the same type of elements-metal or nonmetal atoms. Due to the distinct electronic structures of metal and nonmetal atoms, it is difficult to confer the properties of metals, such as high thermal/electrical conductivity to polymers. Although doped conducting polymers[6] have been developed, the scopes of their potential properties are still limited.[7] Constructing the backbones of polymers with metal atoms is an attractive strategy to develop materials that may combine the advantages of both metals and polymers. However, to the best of our knowledge, there are few related studies reported so far owing to the great challenges associated with their synthesis because the weak bonds between metal atoms are unable to stabilize the backbones of polymers as the nonmetal elements do for conventional polymers.[8]

Here, metal atoms are interconnected as the backbones of polymers to yield metal-backboned polymers (MBPs) (Figure 1). As a demonstration, the nickel element is selected. Rational design of multidentate ligands synthesized via an iterative approach led to the successful construction of a series of nickel-backboned polymers (NBPs) with well-defined lengths. The NBPs with 21 nickel atoms were synthesized and can be further extended by tunning the lengths of monomer or end-capping block as well as the number of iteration cycles. This synthetic strategy is also potentially extendable to other transition metals such as copper and cobalt. Interestingly, the Ni–Ni bond length contracted as the extension of NBPs length, resulting in the strengthened Ni–Ni bonds. Furthermore, we demonstrated that the NBPs exhibited bathochromic shifted absorption spectra and narrow energy band gaps as the length extended, providing potential applications in optoelectronic devices and semiconductors. Additionally, the NBPs were highly thermally stable and had high solution processability.

To construct the MBPs, poly(aminopyridine)s and 4-tert-butylcalix[4]arene were rationally chosen as the building blocks (Figure 1a). Poly(aminopyridine)s were treated as hosts for stabilizing the fragile metal backbones considering the N atoms in pyridine and amine groups can provide bind sites for metal atoms and the distance between the adjacent N-atoms fits well with the length of metal-metal bonds.[9] The 4-tert-butylcalix[4]arene was introduced as an ideal scaffold to bundle and align four poly(aminopyridine) chains

[*] K. Zeng,[+] Y. Yang,[+] J. Xu, N. Wang, J. Xu, Y. Zhang, Y. Wu, Prof. Y. Xu, Prof. G. Wang, Prof. P. Chen, Prof. B. Wang, Prof. X. Sun, Prof. H. Peng
Laboratory of Advanced Materials, State Key Laboratory of Molecular Engineering of Polymers, Department of Macromolecular Science, Fudan University
Shanghai 200438 (P. R. China)
E-mail: gwwang@fudan.edu.cn
penghs@fudan.edu.cn

W. Tang
School of Chemical Engineering, State Key Laboratory of Chemical Engineering, East China University of Science and Technology
Shanghai 200237 (China)

Prof. G. Jin
State Key Laboratory of Molecular Engineering of Polymers, Shanghai Key Laboratory of Molecular Catalysis and Innovative Materials, Department of Chemistry, Fudan University
Shanghai 200438 (P. R. China)

[+] These authors contributed equally to this work.

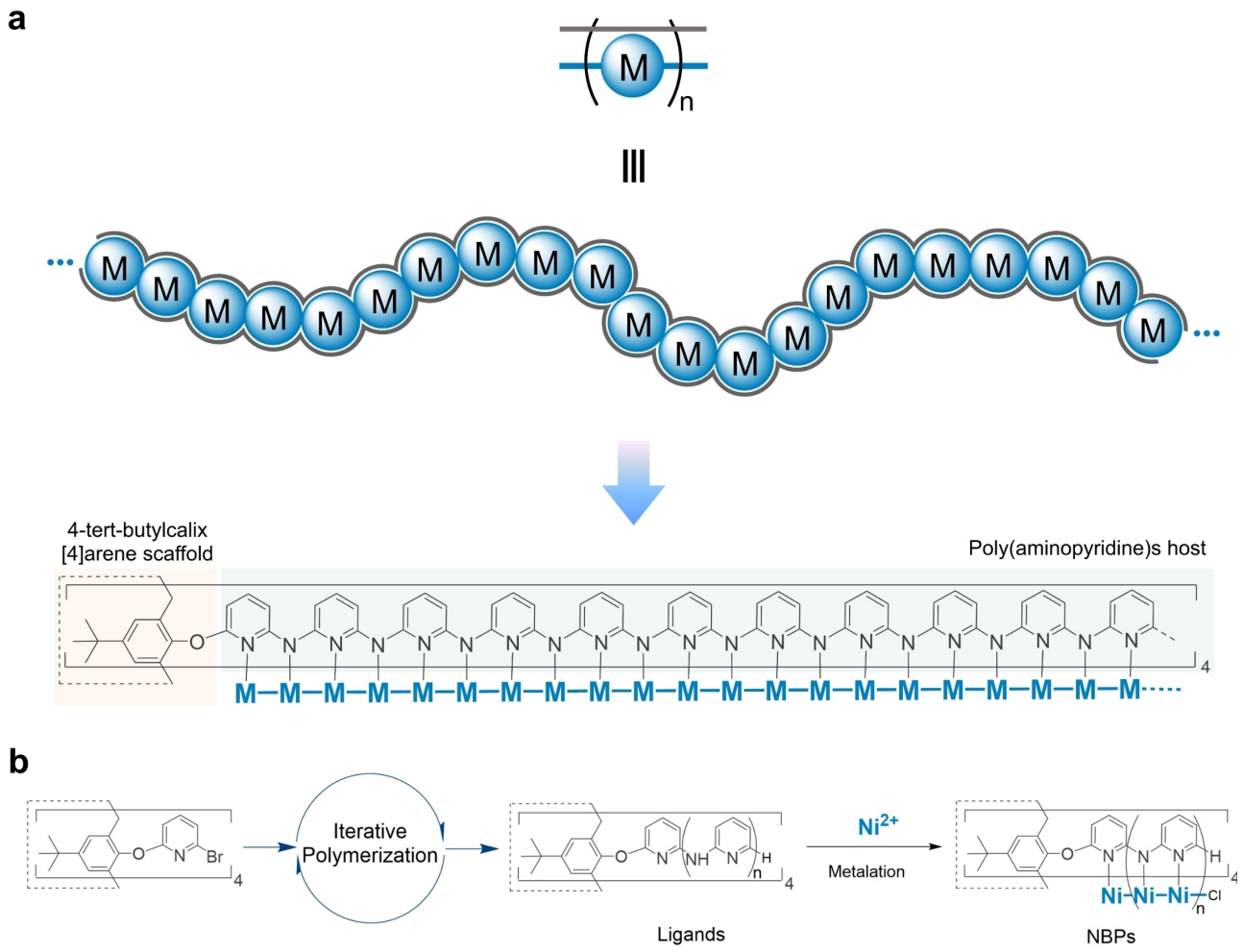

Figure 1. Structure and synthetic approach to MBP. a) Representation of the architecture and the designed molecular structure of MBP. The line in grey represents the ligand and "M" represents the metal atom. b) Synthetic approach to NBPs by metalating metal salt with the ligands synthesized via an iterative polymeric methodology (Scheme S4).

in spatial orientation and geometry that favors the formation of MBPs. Furthermore, an iterative synthetic methodology was developed to extend the poly(aminopyridine)s host in a length-controlled polymerizing manner with convenient purification processes (Scheme S4). The targeted MBPs were then synthesized with well-defined lengths by metalating the resulting ligands with metal ions (Figure 1b).

To check the feasibility of the developed strategy, an NBP with 3 nickel atoms was first synthesized by metalating the corresponding ligand ($n=1$) with nickel ions. Matrix assisted laser desorption/ionization time-of-flight (MALDI-TOF) mass spectrometry analysis showed a parent ion peak for the target product with an isotope pattern in great agreement with the formulation given for this compound (Figure 2a and c). From the Fourier transform infrared (FT-IR) spectroscopy (Figure S1a), the evident stretching vibration peaks of N–H bond at 3266, 3186 and 3103 cm^{-1} together with the bending vibration peaks of N–H bond at 1510 cm^{-1} for the ligand were observed. However, the N–H signals disappeared in the spectrum for the metallic product that showed nearly plat curve at the same regions, consistent with the expected structure of NBP with 3 nickel atoms whose N atoms were all coordinated with nickel atoms. In the Raman spectrum for the metallic product, the peaks at 319, 420–263 and 219 cm^{-1} could be assigned to the Ni–Ni stretching mode $\nu_{Ni\text{-}Ni}$, Ni–N stretching modes $\nu_{Ni\text{-}N}$ and N–Ni–N bending mode $\delta_{N\text{-}Ni\text{-}N}$, respectively (Figure S2).[10] Furthermore, single crystals suitable for X-ray diffraction analysis were obtained and analyzed, which clearly indicated that three nickel atoms were bonded in a linear array with Ni–Ni distances of 2.38–2.39 Å and were helically wrapped by four oligo(aminopyridine)s as expected (Figure 2b and S3). It should be noted that the Ni–Ni distances were shortened by 0.06 Å compared with previously reported trinickel-contained compounds axially ligated with two chloride ions,[11] resulted from the removal of axial chloride ions from the NBP due to the steric hindrance effect of 4-tert-butylcalix[4]arene. Such tendency was consistent with its oxidized species with delocalized Ni–Ni interactions,[12] suggesting the formation of Ni–Ni bonds in NBP.[11] In addition, the Ni–Ni interactions were more obvious in compounds with more nickels.[13] Therefore, the special

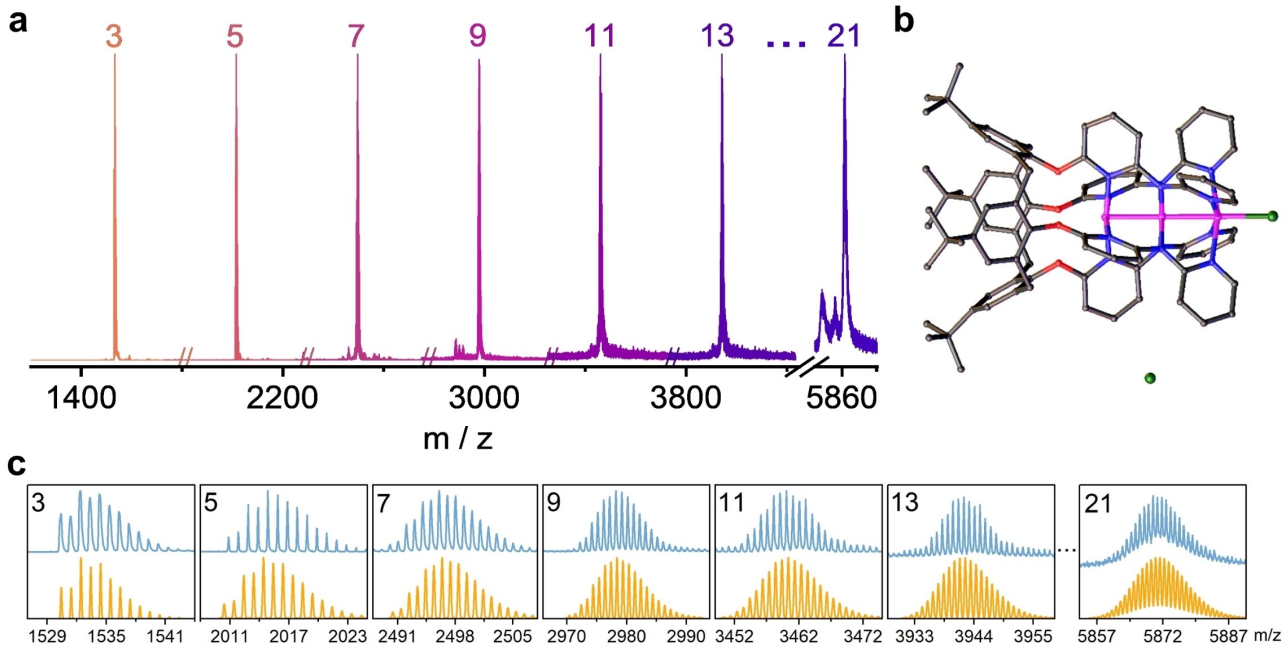

Figure 2. Characterization of NBPs. a) Conjoined MALDI-TOF mass spectra of the NBPs. *m*/*z*, mass/charge ratio. b) Crystallographic structure of NBP with 3 nickel atoms.[14] Carbon atoms are colored in gray, oxygen atoms are colored in red, nitrogen atoms are colored in blue, chlorine atoms are colored in green and nickel atoms are colored in pink. Hydrogen atoms and solvent molecules are omitted for clarity. The lengths of Ni–Ni bonds are 2.38 Å (left) and 2.39 Å (right), respectively. c) Magnified MALDI-TOF mass spectra (top) and simulated isotope pattern (bottom) of NBPs with 3 – 21 nickel atoms. The left top number represents the number of nickel atom.

binding mode of metal atoms in MBPs makes possible the electron delocalization over the whole metal framework, which determines themselves a potential property of electrical conduction.

Having confirmed the structure of NBP with 3 nickel atoms, we further synthesized a series of longer NBPs by the similar method. Taking advantage of the *N,N*-di(dimethoxybenzyl)-protected 2-amino-6-bromopyridine as monomer, ligands with longer lengths were readily synthesized in nearly quantitively yields through the efficient coupling and deprotection cycles, followed by end-capping with 2-bromopyridine. After metalating with nickel ions, a series of longer NBPs were successfully achieved (Figure 2a). Alternatively, monomers or end-capping blocks containing more aminopyridine units were also adoptable, making this synthetic strategy efficient for constructing longer MBPs. As a demonstration, the NBP with 21 nickel atoms was synthesized using five aminopyridine units-containing end-capping block and isolated in high purity (Scheme S5 and Figure S4). These results indicate that this synthesis methodology is feasible and versatile for constructing MBPs with well-defined lengths by tuning the lengths of monomer and end-capping block, as well as the number of iteration cycles, and is extendable to other transition metals such as copper and cobalt (Figure S5). In addition, these NBPs exhibited outstanding solubilities in dichloromethane that was distinct from their precursors and hence can be isolated by simple filtration.

Similar to that for NBP with 3 nickel atoms, isotope patterns observed in MALDI-TOF mass spectra for longer NBPs matched well with the simulated patterns and mass numbers expected for their formulations (Figure 2c). Meanwhile, their structures were further confirmed by FT-IR spectra, in which the stretching vibration peaks of N–H bond at ~3270, 3190 and 3110 cm^{-1} together with the bending vibration peak of N–H bond at ~1510 cm^{-1} disappeared as results of the coordination of nickel atoms with the nitrogen atoms (Figure 3a).

X-ray absorption spectroscopy (XAS) measurements provided further insights into the electronic properties and coordination structures of NBPs. Their ex situ Ni K-edge X-ray absorption near-edge spectroscopy and extended X-ray absorption fine-structure spectroscopy showed similar absorption profiles with that for the reference NiO rather than Ni foil, implying the oxidation state of Ni atoms after metalation (Figure S6 and S7).[15] According to the corresponding Fourier-transformed extended X-ray absorption fine structure spectra (FT-EXAFS, Figure 3b), there was a Ni–Ni contribution at a distance of 2.1 Å in NBP with 3 nickel atoms, which was in great agreement with that in bulk nickel and the Feff calculation results according to its crystal structure (Figure S8). As a comparison, Ni–Ni contributions at slightly shorter distances of ~2.0 Å were revealed in NBPs with more than 3 nickel atoms (Figure 3b). These results indicate that the nickel atoms in the NBPs have been bonded, with distances shorter than that in bulk.

Furthermore, cryogenic transmission electron microscopy (Cryo-TEM) was used to probe the morphologies of NBPs. Cryo-TEM image of a typical NBP with 13 nickel atoms (Figure 3c) showed uniform black strips that were

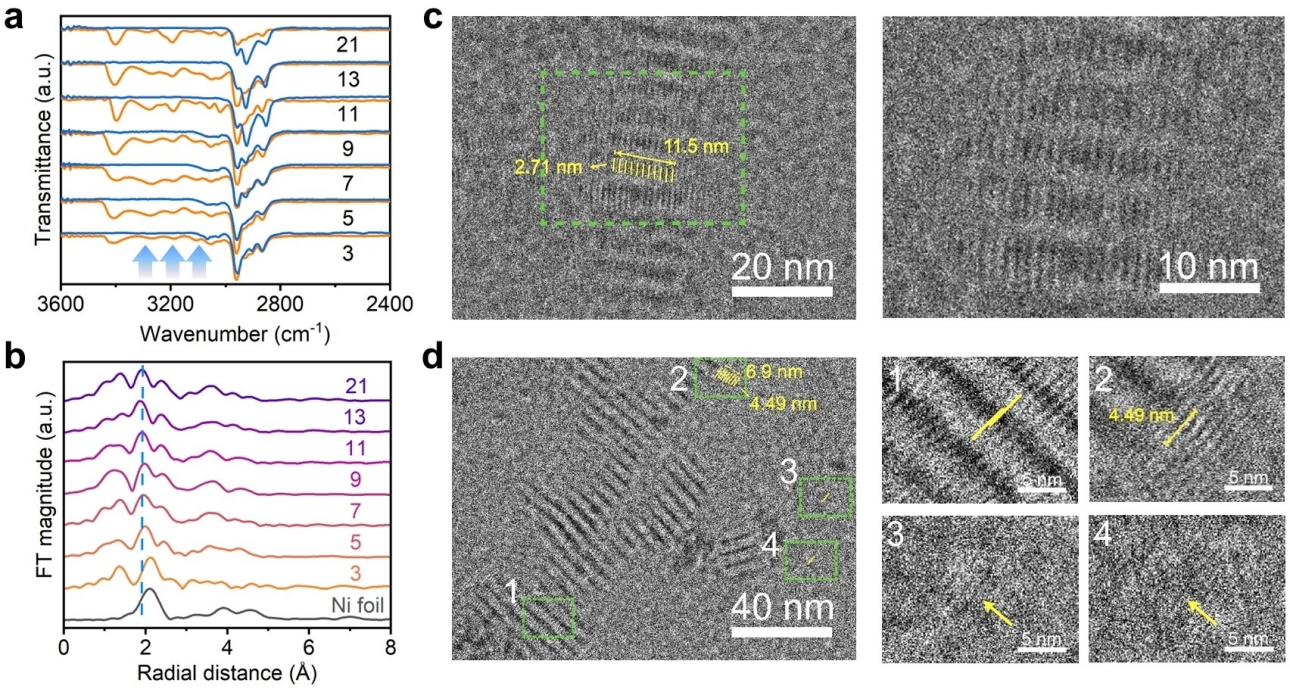

Figure 3. Structure characterization of NBPs. a) Partial FTIR spectra of NBPs with 3 – 21 nickel atoms (in blue) and corresponding ligands (in orange). b) FT-EXAFS spectra of NBPs with Ni foil as reference. c), d) Cryo-TEM images of NBPs with 13 (c) and 21 (d) nickel atoms, respectively. Right images: zoomed portions.

assembled regularly in array. The length and diameter of each black strip were measured as ~2.7 and ~1.2 nm, respectively, in good agreement with those of the predicted structure of NBP with 13 nickel atoms in the backbone (Figure S9a). In the cryo-TEM images for NBP with 21 nickel atoms (Figure 3d), black strips in the single and array distributions were also clearly observed with an identical diameter of ~1.2 nm but longer length of ~4.5 nm compared with the NBP with 13 nickel atoms, also consistent with the calculated results (Figure S9b).

Optical properties of the NBPs were also investigated. Strong absorption bands with molar extinction coefficients typically over $7\times10^4\ M^{-1}\ cm^{-1}$ were observed from the ultraviolet-visible spectroscopy absorption spectra in dichloromethane solution (Figure 4a), corresponding to the π-π* absorption band. With the increase of the number of nickel atom, the maximum absorption wavelengths were bathochromically shifted with gradually increased absorption coefficients, probably attributed to the gradually extended π-electron conjugated structures. Such a tunability of properties renders the NBPs potential applications in optoelectronic devices. Different from absorption results, the fluorescence emission spectra exhibited almost identical profiles (Figure S10). The two main emission peaks at ~405 and ~430 nm together with a shoulder peak at ~450 nm could be attributed to the charge transfer between ligand and nickel atoms.[16]

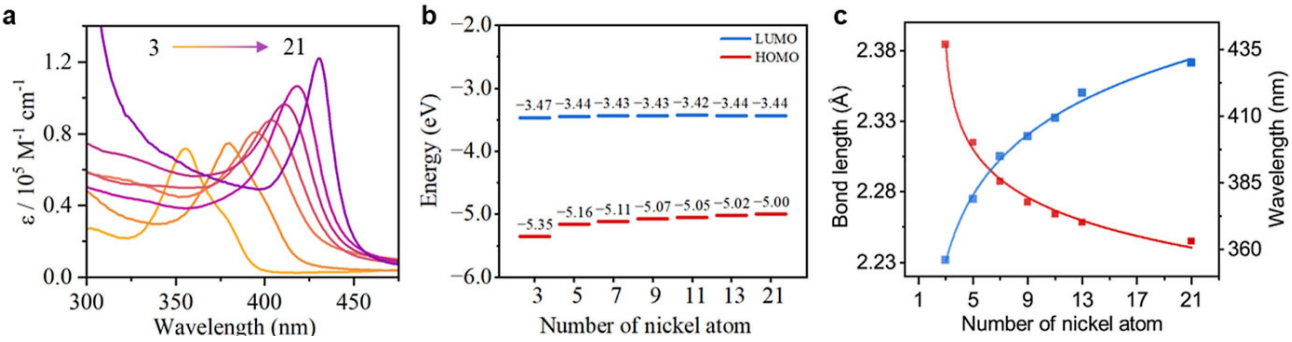

Figure 4. Optical, electrochemical and bond properties of NBPs. a) Ultraviolet-visible spectra of NBPs. b) HOMO and LUMO energies of NBPs. c) The dotted curves give the calculated lengths of Ni–Ni bonds in average (red) and the maximum absorption wavelengths (blue) for NBPs with 3 – 21 nickel atoms, and the fitting results are represented by the solid lines.

Furthermore, the redox properties of NBPs were investigated with cyclic voltammetry (CV) (Figure S11). The CV curve of NBP with 3 nickel atoms exhibited three reversible redox couples at $E_{1/2} = -0.75$, $+0.80$ and $+1.14$ V (vs. Ag/AgCl), respectively. With the increase of the number of nickel atom, the reduction processes remained at the constant potential, indicating their similar electron addition capabilities to the Ni_n^{2n+} cores, while the oxidation potentials were gradually decreased, indicating easier removal of electrons from the antibonding orbitals of longer Ni_n^{2n+} cores and thus the formation of delocalized Ni–Ni bonds.[9] Subsequently, their frontier orbitals were calculated according to the CV results (Figure 4b). All NBPs showed similar lowest unoccupied molecular orbital energies (LUMOs) in a small range of −3.47 to −3.42 eV, while the highest occupied molecular orbital energies (HOMOs) were increased from −5.35 eV for the NBP with 3 nickel atoms to −5.00 eV for the NBP with 21 nickel atoms. As a result, the HOMO–LUMO energy gaps were gradually decreased from 1.88 to 1.56 eV, which is indeed consistent with the observed changes in spectral absorptions as a function of the number of nickel atom. Meanwhile, their optical band gaps were also estimated as 1.56–1.90 eV (Figure S12), which well agreed with the band gaps achieved in CV results both in values and changes. Such narrow and tunable band gaps of NBPs make them promising for the applications of semiconductors.

As the unique one-dimensional helical structure reduced intramolecular π-π stacking, these NBPs showed high solubilities in organic solvents such as dichloromethane even with increased *n* values. As a demonstration, NBP with 21 nickel atoms (100.64 mg) was dissolved in 1.0 mL dichloromethane at room temperature and no precipitation was observed although ca. 80 % solvent evaporated after 48 h (Figure S13), demonstrating the excellent solution processability of NBPs. In addition, the NBPs also show high thermal stability as revealed by the thermogravimetric analysis, with a decomposition temperature onset above 380 °C (Figure S14).

To get insights into the structures of NBPs, theoretical calculations were employed based on the density functional theory (DFT) using Gaussian 09 program package.[17] The calculated Ni–Ni bond lengths for NBP with 3 nickel atoms were 2.38 and 2.39 Å, which agreed with the values measured from its single crystals (2.38–2.39 Å). Interestingly, as the number of nickel atoms increased, the average length of Ni–Ni bonds of NBPs gradually decreased in a trend fitting with the logarithm drawing (Figure 4c), suggesting the contraction of Ni–Ni distances and hence the strengthened Ni–Ni bonds. This contraction may be resulted from the extended p-π conjugation that shortened the C–N distance of ligand and hence the distance of the adjacent N-atoms.[18] This conjugation effect was also evidenced by the bathochromically shifted maximum absorption wavelengths (Figure 4c).

In summary, the metal atoms are interconnected as the backbones to yield MBPs with well-defined lengths in this work. The involved NBPs are demonstrated for excellent optical, electrochemical and thermal properties. This work represents a general and effective strategy to design and synthesize a variety of new functional polymers in the future.

Acknowledgements

This work was supported by STCSM (20JC1414902, 21511104900) and NSFC (22105045, 52122310, 22075050, 52222310, T2222005, 22175042). We acknowledge the Beijing Synchrotron Radiation Facility for provision of synchrotron radiation beamtime at the 1W1B beamline and would like to thank L. Zheng for the assistance with the measurements. We thank B. Zhang, Y. Zeng, Y. Wang, and R. Huang for their assistance.

Conflict of Interest

The authors declare no conflict of interest.

Data Availability Statement

The data that support the findings of this study are available in the Supporting Information of this article.

Keywords: Metal Backbone · Nickel · Polymers · Poly(Aminopyridine)S

[1] a) K. Koner, S. Karak, S. Kandambeth, S. Karak, N. Thomas, L. Leanza, C. Perego, L. Pesce, R. Capelli, M. Moun, M. Bhakar, T. G. Ajithkumar, G. M. Pavan, R. Banerjee, *Nat. Chem.* **2022**, *14*, 507–514; b) Y. Zeng, P. Gordiichuk, T. Ichihara, G. Zhang, E. Sandoz-Rosado, E. D. Wetzel, J. Tresback, J. Yang, D. Kozawa, Z. Yang, M. Kuehne, M. Quien, Z. Yuan, X. Gong, G. He, D. J. Lundberg, P. Liu, A. T. Liu, J. F. Yang, H. J. Kulik, M. S. Strano, *Nature* **2022**, *602*, 91–95; c) A. Charpentier Poncelet, C. Helbig, P. Loubet, A. Beylot, S. Muller, J. Villeneuve, B. Laratte, A. Thorenz, A. Tuma, G. Sonnemann, *Nat. Sustainability* **2022**, *5*, 717–726.

[2] a) Q. Wu, P. M. Rauscher, X. Lang, R. J. Wojtecki, J. J. d Pablo, M. J. A. Hore, S. J. Rowan, *Science* **2017**, *358*, 1434–1439; b) A. K. Mohanty, F. Wu, R. Mincheva, M. Hakkarainen, J. M. Raquez, D. F. Mielewski, R. Narayan, A. N. Netravali, M. Misra, *Nat. Rev. Methods Primers* **2022**, *2*, 46; c) X. Song, B. Bao, J. Tao, S. Zhao, X. Han, H. Liu, *J. Phys. Chem. C* **2019**, *123*, 1828–1838.

[3] a) G. Wu, C. Wang, M. Sun, W. Ding, *J. Magnesium Alloys* **2021**, *9*, 1–20; b) J. Zhang, S. Liu, R. Wu, L. Hou, M. Zhang, *J. Magnesium Alloys* **2018**, *6*, 277–291; c) Y. Shi, B. Yang, P. K. Liaw, *Metals* **2017**, *7*, 43.

[4] E. P. George, D. Raabe, R. O. Ritchie, *Nat. Rev. Mater.* **2019**, *4*, 515–534.

[5] a) R. Balint, N. J. Cassidy, S. H. Cartmell, *Acta Biomater.* **2014**, *10*, 2341–2353; b) Z. Song, Z. Han, S. Lv, C. Chen, L. Chen, L. Yin, J. Cheng, *Chem. Soc. Rev.* **2017**, *46*, 6570–6599; c) F. Vidal, F. Jakle, *Angew. Chem. Int. Ed.* **2019**, *58*, 5846–5870; *Angew. Chem.* **2019**, *131*, 5904–5929; d) M. M. Velencoso, A. Battig, J. C. Markwart, B. Schartel, F. R. Wurm, *Angew. Chem.*

Int. Ed. **2018**, *57*, 10450–10467; *Angew. Chem.* **2018**, *130*, 10608–10626.
[6] H. Shirakawa, E. J. Louis, A. G. MacDiarmid, C. K. Chiang, A. J. Heeger, *J. Chem. Soc. Chem. Commun.* **1977**, *16*, 578–580.
[7] G. Pacchioni, *Nat. Rev. Mater.* **2021**, *6*, 873–873.
[8] a) H. Ohnishi, Y. Kondo, K. Takayanagi, *Nature* **1998**, *395*, 780–783; b) T. Kizuka, *Phys. Rev. B* **2008**, *77*, 155401; c) K. Zeng, H. Peng, *Chin. J. Polym. Sci.* **2023**, *41*, 3–6.
[9] P. J. Chen, M. Sigrist, E. C. Horng, G. M. Lin, G. H. Lee, C. H. Chen, S. M. Peng, *Chem. Commun.* **2017**, *53*, 4673–4676.
[10] a) B. H. Wu, L. Y. Hung, J. Y. Chung, S. M. Peng, I. C. Chen, *J. Phys. Chem. C* **2018**, *122*, 6332–6339; b) B. H. Wu, J. Y. Lin, K. Y. Ho, M. J. Huang, S. A. Hua, M. C. Cheng, Y. W. Yang, S. M. Peng, C. H. Chen, I. C. Chen, *J. Phys. Chem. C* **2016**, *120*, 20297–20302.
[11] F. A. Cotton, C. A. Murillo, Q. Wang, M. D. Young, *Eur. J. Inorg. Chem.* **2008**, 5257–5262.
[12] J. F. Berry, F. A. Cotton, L. M. Daniels, C. A. Murillo, *J. Am. Chem. Soc.* **2002**, *124*, 3212–3213.
[13] J. F. Berry, F. A. Cotton, P. Lei, T. Lu, C. A. Murillo, *Inorg. Chem.* **2003**, *42*, 3534–3539.
[14] Deposition Number 2214751 (for NBP with 3 nickel atoms) contain the supplementary crystallographic data for this paper. These data are provided free of charge by the joint Cambridge Crystallographic Data Centre and Fachinformationszentrum Karlsruhe Access Structures service.
[15] a) B. Zhang, L. Wang, Z. Cao, S. M. Kozlov, F. P. García de Arquer, C. T. Dinh, J. Li, Z. Wang, X. Zheng, L. Zhang, Y. Wen, O. Voznyy, R. Comin, P. De Luna, T. Regier, W. Bi, E. E. Alp, C. W. Pao, L. Zheng, Y. Hu, Y. Ji, Y. Li, Y. Zhang, L. Cavallo, H. Peng, E. H. Sargent, *Nat. Catal.* **2020**, *3*, 985–992; b) B. Qiao, A. Wang, X. Yang, L. F. Allard, Z. Jiang, Y. Cui, J. Liu, J. Li, T. Zhang, *Nat. Chem.* **2011**, *3*, 634–641; c) Y. Li, C. K. Peng, H. Hu, S. Y. Chen, J. H. Choi, Y. G. Lin, J. M. Lee, *Nat. Commun.* **2022**, *13*, 1143.
[16] a) P. Herr, C. Kerzig, C. B. Larsen, D. Häussinger, O. S. Wenger, *Nat. Chem.* **2021**, *13*, 956–962; b) C. Diner, K. J. Szabó, *J. Am. Chem. Soc.* **2017**, *139*, 2–14; c) P. Chábera, Y. Liu, O. Prakash, E. Thyrhaug, A. E. Nahhas, A. Honarfar, S. Essén, L. A. Fredin, T. C. B. Harlang, K. S. Kjær, K. Handrup, F. Ericson, H. Tatsuno, K. Morgan, J. Schnadt, L. Häggström, T. Ericsson, A. Sobkowiak, S. Lidin, P. Huang, S. Styring, J. Uhlig, J. Bendix, R. Lomoth, V. Sundström, P. Persson, K. Wärnmark, *Nature* **2017**, *543*, 695–699.
[17] Gaussian 09, Revision A. 2, G. T. M. Frisch, H. B. Schlegel, G. E. Scuseria, M. A. Robb, J. R. Cheeseman, G. Scalmani, V. Barone, B. Mennucci, G. Petersson, Gaussian, Inc., Wallingford CT, **2009**.
[18] H. Zhang, X. Jiang, W. Wu, Y. Mo, *Phys. Chem. Chem. Phys.* **2016**, *18*, 11821–11828.

Manuscript received: November 1, 2022
Accepted manuscript online: January 14, 2023
Version of record online: January 31, 2023